The Subsurface Stress Field Caused by Both Normal Loading and Tangential Loading

Young-Pil Koo*
Mechanical Material & Parts Center Busan Techno-Park, Geumjeong-gu, Busan 609-735, Korea
Tae-Wan Kim
Nanotribology Laboratory, Ohio State University, Geumjeong-gu, Busan 609-735, Korea
Yong-Joo Cho
School of Mechanical Engineering, Pusan National University, Geumjeong-gu, Busan 609-735, Korea

The subsurface stress field caused by both normal loads and tangential loads has been evaluated using the rectangular patch solution. The effect of tangential loading on the subsurface stress field has been investigated in detail for both the cylinder-on-cylinder contact and a spur gear teeth contact. For the cylinder-on-cylinder contact, the subsurface stress fields are moved more to the direction of tangential loads and the positions where the maximum stress occur are getting closer to the surface with the increasing tangential loads. The subsurface stress fields of the gear teeth contact are expanded more widely to the direction of tangential loads with the increasing tangential loads. The friction coefficient of a gear teeth contact is low because they are operated in a lubricated condition, and therefore surface tractions in the EHL condition hardly affect on the subsurface stress field.

Key Words : Subsurface Stress, Tangential Load, Elasto-hydrodynamic Lubrication, Spur Gear

Nomenclature

a : Half size of a rectangular patch in sliding (x) direction
b : Half size of a rectangular patch in transeverse (y) direction
f_c : Friction coefficient
n : Number of rectangular patches
p : Normal load or surface pressure
p_0 : Maximum Hertzian contact pressure
q : Tangential load
r : Contact-radius or semi-width of the contact area
s_{ij} : Subsurface stress components caused by normal load
t_{ij} : Subsurface stress components caused by tangential load
V : Velocity of lubricant
W : Total normal load
x, y, z : Cartesian coordinates for the stress in the body
Γ, Λ : Potential functions for normal loads
Ω, Ω_1 : Potential functions for tangential loads
ξ, ς : Cartesian coordinates for the loads on a surface
η : Viscosity of lubricant
τ_1 : Maximum shear stress
σ_e : Von Mises' effective stress
σ_{ij} : Combined subsurface stress components

* Corresponding Author,
E-mail : kyp@mechamap.or.kr
TEL : +82-51-510-3754; **FAX** : +82-51-512-3587
Mechanical Material & Parts Center Busan Techno-Park, Geumjeong-gu, Busan 609-735, Korea. (Manuscript **Received** October 8, 2004; **Revised** March 23, 2005)

1. Introduction

Machines need normally relative motions between their components to produce profitable work. The contact surface of mechanical components is both the interface of the relative motion and medium of power transmission. Most breakdowns in machines are mainly caused by damage of the contact surface and therefore, lifetime of machinery is very dependent on the reliability of the contact surface (Rabinowicz, 1995). Not only a macroscopic strength but also a microscopic stress field should be considered in designing reliable surfaces. Because the load on the surface generates subsurface stresses, an actual loading condition should be known prior to a subsurface stress analysis and a suitable analysis method should be chosen.

Many studies have been done on the analysis of the subsurface stress. Exact solutions were derived for the simple contact contour of a circle or an ellipse (Hertz, 1896). Potential functions were adopted to obtain the subsurface stress field of general contact contours (Cerruti, 1882; Boussinesq, 1885). This method was combined with a numerical method. The surface endowed with normal loads was divided into many tiny rectangular patches and discrete numerical solutions were applied on all patches to obtain a subsurface stress field (Love, 1929). For the subsurface stress field caused by a tangential load, numerical solutions and analytic solutions were introduced (Kalker, 1986; Ahmadi et al., 1987). To improve accuracy of solutions, amended solutions were introduced (Yu et al., 1996). More accurate solutions were derived for the subsurface stress distribution caused by a tangential load by using both the potential functions and rectangular patches (Cho et al., 2000a). For the purpose of obtaining accurate solutions rapidly, several new methods have been developed lately: Fourier transform and numerical integration (Elsharkawy, 1999), fast Fourier transform (Cho et al., 2000b; Peng et al., 2001), and Flament equation and numerical integration (Mihailidis, 2001) etc. The method of using potential functions and rectangular patches provides numerical solutions that are very close to exact solutions (Cho et al., 2000a).

The former researches on the subsurface stress field of authors were focused on either tangential loading or normal loading itself. In the present research, the subsurface stress field caused by both normal loads and tangential loads has been evaluated using the rectangular patch solution. Especially, the influence of tangential loading on the subsurface stress field has been investigated in detail for both the cylinder-on-cylinder contact without lubrication and a spur gear teeth contact with elasto-hydrodynamic lubrication.

2. Subsurface Stress Field

When both a normal load and a tangential load acts on a surface, as shown in Fig. 1, subsurface stresses will be superposition of stresses caused by each load. If multiple loads are imposed on the surface, the subsurface stress field can be obtained by accumulating the contribution of whole loads on the stress field. Namely, Eq. (1) expresses the stress components of an arbitrary point 'A' in the body.

$$\sigma_{ij}=\sum_{k=1}^{n}(s_{ij}+t_{ij})_k \tag{1}$$

where, s_{ij}: stress components caused by the normal load, t_{ij}: stress components caused by the tangential load, n: number of rectangular patches on where loads are imposed,

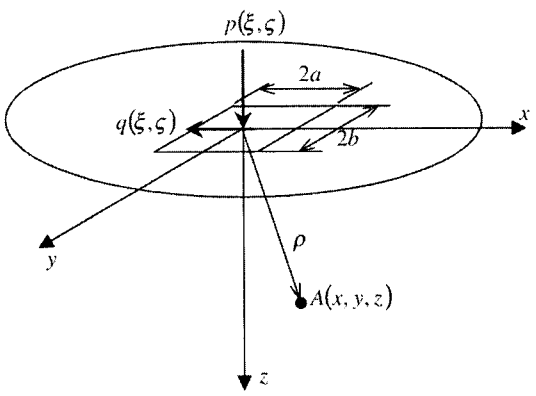

Fig. 1 Loading on surface and coordinate system

$$i=1, 2, 3, j=1, 2, 3$$

Potential functions for normal loads are defined by Eq. (2) and stress components by normal loads are shown in Eq. (3) (Love, 1929).

$$\Gamma=\iint p\log(z+p)\,d\xi d\zeta$$
$$\Lambda=\iint \frac{p}{l}\,d\xi d\zeta \tag{2}$$

where,

$$\rho=\sqrt{(x-\xi)^2+(y-\zeta)^2+z^2}$$

$$s_{11}=\frac{1}{2\pi}\left(\frac{\lambda}{\lambda+G}\frac{\partial\Lambda}{\partial z}-\frac{G}{\lambda+G}\frac{\partial^2\Gamma}{\partial x^2}-z\frac{\partial^2\Lambda}{\partial x^2}\right)$$
$$s_{22}=\frac{1}{2\pi}\left(\frac{\lambda}{\lambda+G}\frac{\partial\Lambda}{\partial z}-\frac{G}{\lambda+G}\frac{\partial^2\Gamma}{\partial y^2}-z\frac{\partial^2\Lambda}{\partial y^2}\right)$$
$$s_{33}=\frac{1}{2\pi}\left(\frac{\partial\Lambda}{\partial z}-z\frac{\partial^2\Lambda}{\partial z^2}\right)$$
$$s_{12}=\frac{1}{2\pi}\left(\frac{G}{\lambda+G}\frac{\partial^2\Gamma}{\partial x\partial y}+z\frac{\partial^2\Lambda}{\partial x\partial y}\right) \tag{3}$$
$$s_{23}=\frac{1}{2\pi}\left(z\frac{\partial^2\Lambda}{\partial y\partial z}\right)$$
$$s_{31}=\frac{1}{2\pi}\left(z\frac{\partial^2\Lambda}{\partial z\partial x}\right)$$

where,

$$\lambda=\frac{Ev}{(1+v)(1-2v)},\quad G=\frac{E}{2(1+v)}$$

For tangential loads, Eqs. (4), (5) are potential functions and Eq. (6) expresses stress components caused by tangential loads.

$$\Phi_1=\iint q\{z\ln(\rho+z)-\rho\}d\xi d\zeta \tag{4}$$

$$\Phi=\frac{\partial\Phi_1}{\partial z}=\iint q\ln(\rho+z)\,d\xi d\zeta \tag{5}$$

$$t_{11}=\frac{v+1}{\pi}\frac{\partial^2\Phi}{\partial x\partial z}+\frac{1}{2\pi}\left\{2v\frac{\partial^3\Phi_1}{\partial x^3}-z\frac{\partial^3\Phi}{\partial x^3}\right\}$$
$$t_{22}=\frac{v}{\pi}\frac{\partial^2\Phi}{\partial x\partial z}+\frac{1}{2\pi}\left\{2v\frac{\partial^3\Phi_1}{\partial x\partial y^2}-z\frac{\partial^3\Phi}{\partial x\partial y^2}\right\}$$
$$t_{33}=-\frac{z}{2\pi}\frac{\partial^3\Phi}{\partial x\partial z^2} \tag{6}$$
$$t_{12}=\frac{1}{2\pi}\left\{\frac{\partial^2\Phi}{\partial z\partial y}+2v\frac{\partial^3\Phi_1}{\partial x^2\partial y}-z\frac{\partial^3\Phi}{\partial x^2\partial y}\right\}$$
$$t_{23}=-\frac{z}{2\pi}\frac{\partial^3\Phi}{\partial x\partial y\partial z}$$
$$t_{31}=\frac{1}{2\pi}\left\{\frac{\partial^2\Phi}{\partial z^2}-z\frac{\partial^3\Phi}{\partial x^2\partial z}\right\}$$

To evaluate stress components in Eqs. (3), (4), partial derivatives should be known in advance. They are available from Love's solution for the normal load (1929) and Cho et al.'s for the tangential load (2000a).

3. Analysis Object and Conditions

3.1 Cylinder-on-cylinder contact

For the comparison of subsurface stress fields with and without tangential load, cylinder on cyliner dry contact model is adopted. The analysis procedures are: First, the contact surface is devided into many tiny rectangular patches. The contact analysis is performed and the contact pressure, a normal load on the each rectangular patch, is obtained. Tangential loads are defined by multiplication of the normal loads and the friction coeffitient as shown in Eq. (7). Next, the subsurface stresses are calculated by making use of Eqs. (1), (3), and (6).

Though there is no frictions in an ideal cylinders' contact, tangential loads are applied on the contact surface eqivalent to the friction coefficient of 0.1, 0.2, 0.3, and 0.4 for the comparison.

$$q=f_c p \tag{7}$$

3.2 Spur gear teeth contact

Because gears are important mechanical elements which transmit power via contact of gear teeth and are operated in a lubricated condition, it could be valuable study to analyze a subsurface stress field considering these actual operating conditions. The surface of gear teeth in contact is in an elasto-hydronamic lubrication (EHL) condition therefore, the surface pressure is obtainable through the EHL analysis (Koo, 2004). The EHL analysis was performed in the condition of the external load of 1540 N and entraining velocity of

2.94 m/s and the clearance geometry of Fig. 2. Fig. 3 illustrates pressure distribution on the contact surface of gear teeth in the EHL condition. The maximum pressure near tooth edge is 736 MPa, the maximum pressure at tooth center is 659 MPa. Asymmetry of the pressure profile given in Fig. 3 in y-direction is caused by the differences in clearances between two surfaces in the direction.

The surface pressures is considered as normal loads acting on rectangular patches for the subsurface stress analysis.

The friction coefficient in an EHL condition is defined by Eq. (8), which is the ratio of a viscous traction force to a normal force.

$$f_c=\frac{\iint \eta \frac{dV}{dz} dxdy}{W} \tag{8}$$

In addition to this, friction coefficients of 0.1, 0.2, and 0.3 are taken so as to demonstrate lubrication failures. Hertzian contact pressure in the gear teeth contact, in the case that it is assumed as cylinder on cylinder contact, is 592 MPa, which will be used as a reference value of the dimensionless stress in this study.

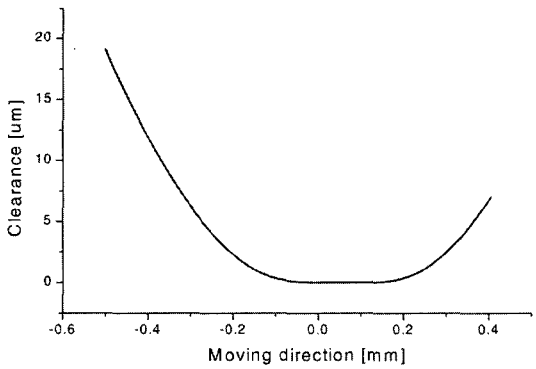

Fig. 2 Clearance geometry of gear teeth

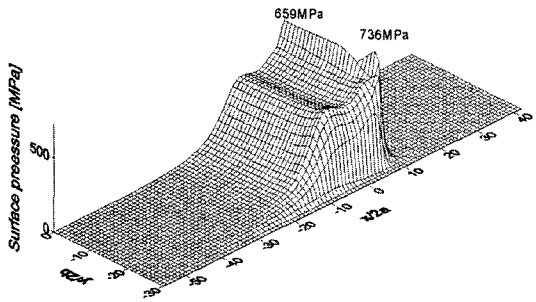

Fig. 3 3-D view of surface pressure on the contacting gear teeth

4. Analysis Results and Discussions

4.1 Cylinder-on-cylinder contact

According to the Hertz theory, the contact of two long cylinders can be summarized in Eq. (9), which means that the maximum shear stress is 0.3 times of the maximum contact pressure and the position of the maximum shear stress is 0.78 times of the semi-contact-width below the surface (Johnson, 1985).

$$\tau_1=0.30p_0 \quad @ \quad x=0,\ z=0.78r \tag{9}$$

The maximum shear stress is calculated by:

$$\tau_1=\sqrt{\left(\frac{\sigma_{33}-\sigma_{11}}{2}\right)^2+\sigma_{31}^2} \tag{10}$$

Fig. 4(a), which is a result of subsurface stress analysis for the Hertzian contact of cylinders, indicates the contour plot of the stress on the plane of the center section. The analysis rersults show that the maximum shear stress is $0.301p_0$ and the depth where the maximum shear stress occurs is $0.775r$, that are very close to Hertzian exact solutions. Fig. 4(b) is a result of subsurface stress analysis for both the normal pressure of Hertzian contact and surface tractions eqivalent to the friction coefficient of 0.1. The maximum shear stress has been increased to $0.306p_0$ due to the superposition of the tangential loading effect on the normal loading effect. The position where the maximum shear stress occurs has been moved to the direction of the tangential load by $0.35r$.

Figures 4(a)-4(e) demonstrate that the position of the maximum shear stress in depth direction is getting closer to the surface with increasing tangential loads. Their relations are summarized in Table 1.

4.2 Spur gear teeth contact

Figure 5(a) is a contour plot of the subsurace stress field on the plane of the center section for normal loads only in the EHL condition, whereas

Fig. 5(b) is the one for both normal loads and surface tractions equivalent to the friction coefficient of 0.025 in the EHL condition. Stresses are normalized values to the maximum Hertzian pressure, p_0, of the line contact. The dimensionless parameter of the length, r, is the semi-width of the Hertzian contact area.

Because the surface pressure in the EHL condition is nonsymmetric and a peak pressure emerges at the downstream of lubricant like Fig. 3, the subsurface stress distribution of Fig. 5(a) is quite different to that of Fig. 4(a). The maximum value of shear stresses is $0.274p_0$ and the position where the maximum stress occurs is $x=0.805r$ and $z=0.251r$. Though the contour plot of Fig. 5(b) shows that the stress pattern has been expanded slightly toward the direction of tangential loads, the friction coefficient in an EHL condition is so low that there is little differences in the values of maximum shear stresses between Fig. 5(a) and Fig. 5(b).

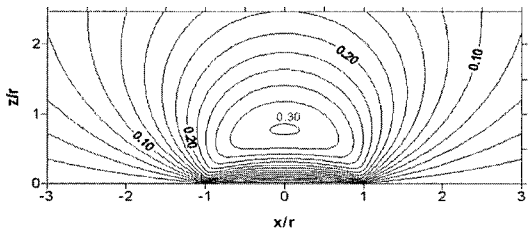

(a) Normal load only, $f_c=0$

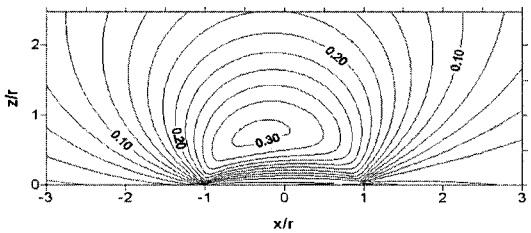

(b) Normal and tangential load, $f_c=0.1$

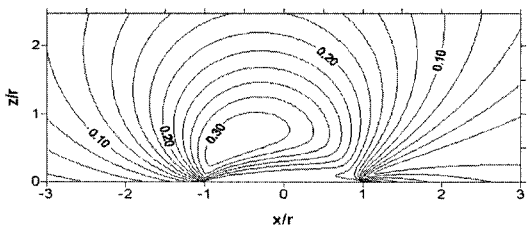

(c) Normal and tangential load, $f_c=0.2$

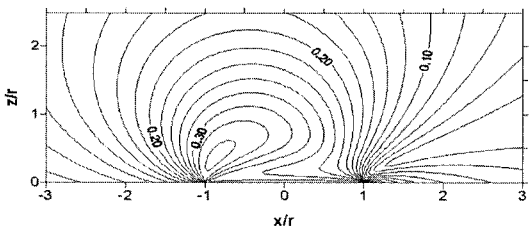

(d) Normal and tangential load, $f_c=0.3$

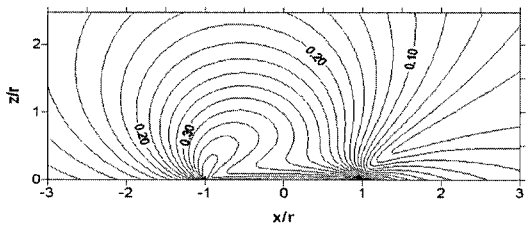

(e) Normal and tangential load, $f_c=0.4$

Fig. 4 Contour of maximum shear stress for the cylinder-on-cylinder contact

Table 1 Maximum shear stresses and their positions

Friction coefficient, f_c	0	0.1	0.2	0.3	0.4
Max. shear stress, τ_1/p_0	0.301	0.306	0.320	0.346	0.403
Position in sliding, x/r	0.	−0.35	−0.60	−0.85	−1.00
Position in depth, z/r	0.775	0.725	0.600	0.375	0.025

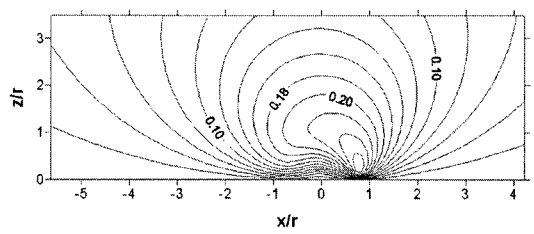

(a) Normal load only, $f_c=0$

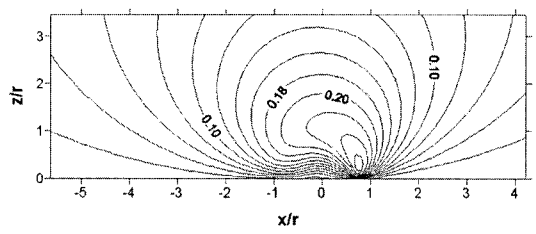

(b) Normal and tangential load, $f_c=0.025$

Fig. 5 Contour of maximum shear stress for the gear teeth contact

Reliablity of machanical elements is influenced by the subsurface stress distribution. To evaluate stress conditions for the gear teeth contact, von Mises' effective stress which is shown in Eq. (11) is introduced.

$$\sigma_e=\sqrt{3(\sigma_{12}^2+\sigma_{23}^2+\sigma_{31}^2)+\frac{1}{2}[(\sigma_{11}-\sigma_{22})^2+(\sigma_{22}-\sigma_{33})^2+(\sigma_{33}-\sigma_{11})^2]} \quad (11)$$

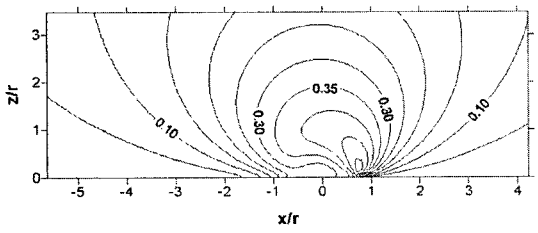

(a) $f_c=0$

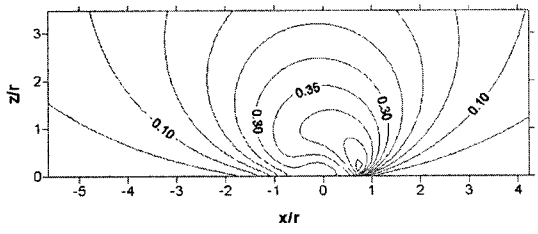

(b) $f_c=0.025$

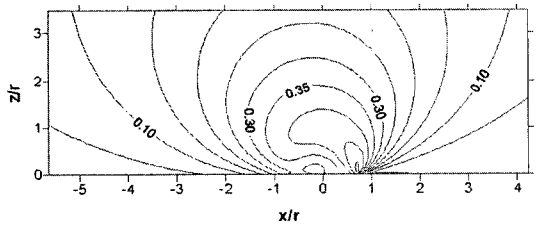

(c) $f_c=0.1$

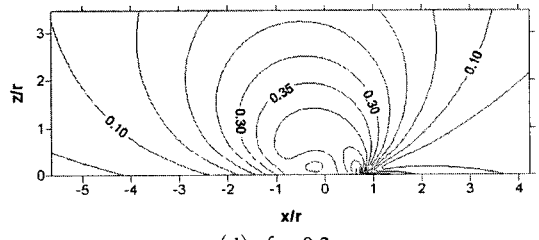

(d) $f_c=0.2$

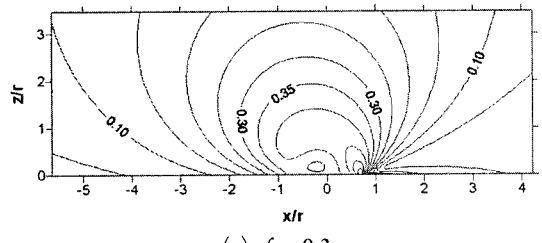

(e) $f_c=0.3$

Fig. 6 Contour of effective stress on the central section

Contour plots of subsurface stresses on the plane of the center section are presented in Fig. 6. Fig. 6(a) is for normal loads in the EHL condition, Fig. 6(b) is for normal loads with tractions in the EHL condition. In Fig. 6(a), the maximum effective stress is $0.512p_0$ and its position is $x=0.704r$, $z=0.201r$. In Fig.6(b), the maximum effective stress is $0.514p_0$ and its position is $x=0.704r$, $z=0.201r$. Because the friction coefficient in the EHL condition is as low as 0.025, the effect of the tangential loading on the subsurface stress is insignificant, whereas the overall contour maps of the iso-stresses have been expanded to the direction of tangential loads slightly.

Because failures of surfaces are mainly resulted from awkward situations like no lubricant supply or irreglarities of surface topology, bigger tangential loads have been applied to simulate these conditions and to investigate the effect of increasing friction coefficients. Figs. 6(c)-6(e) are the analysis results for both normal loads in the EHL condition and tangential loads equvalent to the friction coefficient of 0.1, 0.2, and 0.3 respectively. These figures show that the contour area expands toward the direction of tangential loads more widely with the increasing friction coefficient. Because the increase of the friction coefficient under the same normal loads means the increase of tangential loads, the maximum effective stress is enlarged with the increasing friction coefficient. Moreover, position of the maximum stress is closer to the surface with the enlarged tangential load. The reason of this phenomenon may be related to that the direction of a resultant force, which is the vector sum of a normal load with a tangential load is more inclined toward surface with the increasing tangential load. Therefore, enlargement of tangential loads can adversly affect lifetime of the surface.

Figure 7 indicates contour plot of the stress on the plane of planar section where the maximum effective stress occurs. The maximum stress emerges near edges on where the maximum surface

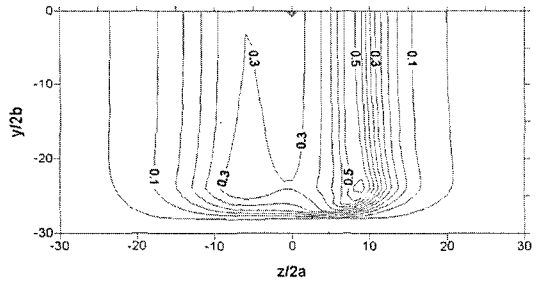

(a) Normal load only, f_c=0

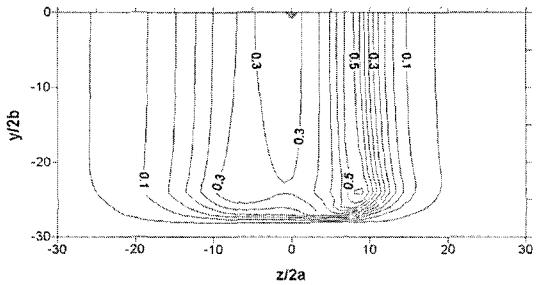

(b) Normal and tangential load, f_c=025

Fig. 7 Contour of effective stress on the plane section

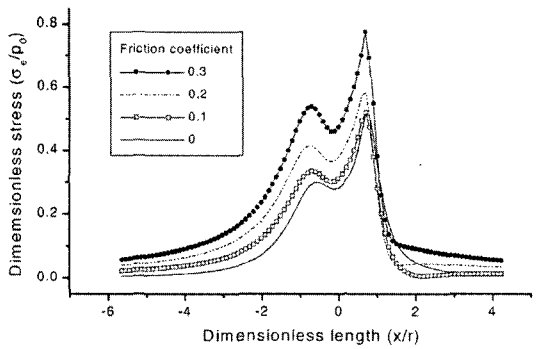

(a) Effective stress

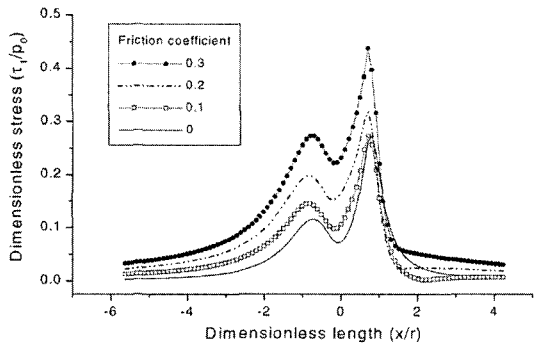

(b) Maximum shear stress

Fig. 8 Profile of stresses at the center of the plane section

pressure acts.

Figure 8(a) is a plot of sectional curves of effective stresses for several friction coefficients. The higher friction coefficients, the bigger the values of subsurface stresses. The subsurface stress fields are clearly expanded more to the direction of tangential load with the increasing friction coefficients. Fig. 8(b), a plot of sectional curves of shear stresses, illustrates the same tendencies as Fig. 8(a).

In the case that the friction coefficient is below 0.1 the effect of tangential loading is not so important therefore, friction force in a lubricated condition would not be harmful to lifetime of the mechanical components.

5. Conclusions

The subsurface stress field caused by both normal loads and tangential loads has been evaluated using the rectangular patch solution. The effect of tangential loading on the subsurface stress field has been investigated in detail for both the cylinder-on-cylinder contact and a spur gear teeth contact.

For the cylinder-on-cylinder contact, the subsurface stress fields are moved more to the direction of tangential loads and the positions where the maximum stress occur are getting closer to the surface with the increasing tangential loads. The subsurface stress fields of the gear teeth contact are expanded more widely to the direction of tangential loads with the increasing tangential loads. The friction coefficient of a gear teeth contact is low because they are operated in a lubricated condition, and therefore surface tractions in the EHL condition hardly affect on the subsurface stress field.

References

Ahmadi, N., Keer, L. M., Mura, T. and Vithoontien, V., 1987, "The Interior Stress Field Caused by Tangential loading of a Rectangular Patch on an Elastic Half Space," *ASME J. of Tribology*, Vol. 109, pp. 627~629.

Boussinesq, J., 1885, Application de Potentials

a l'etude de l'equilibr et du mouvement des solids e'lastiques. Paris : G authier-Villars. 45, p. 108.

Cerruti, V., 1882, Acc. Lincei. Mem.fis. mat., Roma. 13, p. 81.

Cho, Y.-J., Lee, M.-J. and Koo, Y.-P., 2000a, "The Stress Field in the Body by Tangential Loading of a Rectangular Patch on a Semi-Infinite Solid," *KSME, (in Korean), Series A*, Vol. 24, No. 4, pp. 1032~1038.

Cho, Y.-J., Koo, Y.-P. and Kim, T.-W., 2000b, "A New FFT Technique for the Analysis of Contact Pressure and Subsurface Stress in a Semi-Infinite Solid," *KSME International J.*, Vol. 14, No. 3, pp. 331~337.

Elsharkawy, A. A., 1999, "Effect of Friction on Subsurface Stresses in Sliding Line Contact of Multilayered Elastic Solids," *International J. of Solids and Structures*, Vol.36, pp. 3903-3915.

Hertz, H., 1896, Miscellaneous Papers on the Contact of Elastic Solids, Translated by D. E. Johns, McMillan, London.

Johnson, K. L., 1985, Contact mechanics, Chap. 4, pp. 90-104, Cambridge university press.

Kalker, J. J., 1986, "Numerical Calculation of the Elastic Field in a Half-Space," Communications in Applied Numerical Method, Vol. 200, pp. 401~410.

Koo, Y.-P., 2004, "Transient EHL Analysis on Spur Gear Teeth with Consideration of Gear Kinematics," *KSME International J.*, Vol. 18, No. 8, pp. 1319~1326.

Love, A. E. H., 1929, "Stress Produced in a Semi-Infinite Solid by Pressure on Part of the Boundary," Phil. Trans. Royal Society, A228, pp. 377~420.

Mihailidis, A., Bakolas, V. and Drivakos, N., 2001, "Subsurface Stress Field of a Dry Line Contact," *Wear*, Vol. 249, pp. 546~556.

Peng, W. and Bhushan, B., 2001, "Three-dimensional Contact Analysis of Layered Elastic/Plastic Solids with Rough Surfaces," *Wear*, Vol. 249, pp. 741~760.

Rabinowicz, E., 1995, Friction and Wear of Materials, Chap. 1, pp. 5-6, John Wiley & Sons, Inc.

Yu, M. M. -H. and Bhushan, B., 1996, "Contact Analysis of Three-dimensional Rough Surfaces Under Frictionless and Frictional Contact," *Wear*, Vol. 200, pp. 265~280.